



RESEARCH ARTICLE

Extraocular muscle function is impaired in *ryr3*^{-/-} mice

Jan Eckhardt^{1,2}, Christoph Bachmann^{1,2} , Marijana Sekulic-Jablanovic² , Volker Enzmann^{3,4} , Ki Ho Park⁵, Jianjie Ma⁵, Hiroshi Takeshima⁶, Francesco Zorzato^{1,2,7*}, and Susan Treves^{1,2,7*} 

Calcium is an ubiquitous second messenger mediating numerous physiological processes, including muscle contraction and neuronal excitability. Ca²⁺ is stored in the ER/SR and is released into the cytoplasm via the opening of intracellular inositol trisphosphate receptor and ryanodine receptor calcium channels. Whereas in skeletal muscle, isoform 1 of the RYR is the main channel mediating calcium release from the SR leading to muscle contraction, the function of ubiquitously expressed ryanodine receptor 3 (RYR3) is far from clear; it is not known whether RYR3 plays a role in excitation–contraction coupling. We recently reported that human extraocular muscles express high levels of RYR3, suggesting that such muscles may be useful to study the function of this isoform of the Ca²⁺ channel. In the present investigation, we characterize the visual function of *ryr3*^{-/-} mice. We observe that ablation of RYR3 affects both mechanical properties and calcium homeostasis in extraocular muscles. These changes significantly impact vision. Our results reveal for the first time an important role for RYR3 in extraocular muscle function.

Introduction

RYRs are intracellular calcium channels mediating calcium release from ER/SR intracellular calcium stores (Takeshima et al., 1989; Zorzato et al., 1990). Three main isoforms of RYRs encoded by different genes sharing an overall amino acid identity of ~65% have been identified in vertebrates (Ogawa et al., 2000; Meissner, 2017). In skeletal muscle, RYR1 is mostly located on the terminal cisternae junctional face membrane, where it is involved in excitation–contraction coupling (ECC), the process whereby a change in membrane potential is converted into calcium release, leading to muscle contraction (Endo, 1977; Takeshima et al., 1989; Zorzato et al., 1990; Ríos and Pizarro, 1991). RYR2 is predominantly expressed in the cardiac muscle SR, where it is activated by a process called CICR, leading to repetitive contractions of the heart (Bers, 2002). RYR3 is ubiquitously expressed on ER/SR membranes, with high levels of expression in the central nervous system, smooth muscle cells, and developing muscles (Giannini et al., 1992, 1995; Clark et al., 2010; Vaithianathan et al., 2010).

In skeletal and cardiac muscles, RYR1 and RYR2 are either directly coupled to or in close proximity to the dihydropyridine receptor (DHPR; Ríos and Pizarro, 1991; Franzini-Armstrong and

Jorgensen, 1994; Protasi et al., 2000; Bers, 2002). A coupling partner has not been identified for RYR3, though it has been suggested that RYR3 may act as an amplifier and release Ca²⁺ by a CICR mechanism (Protasi et al., 2000; Yang et al., 2001). Lower vertebrates such as fish, frogs, and birds express both RYR1 (referred to as α RYR) and RYR3 (referred to as β RYR) in their skeletal muscles (Airey et al., 1990; Percival et al., 1994). In contrast to α RYRs, which are located on the junctional face membrane, β RYRs are expressed parajunctionally, where they cannot support ECC but are involved in the generation of Ca²⁺ sparks (Perni et al., 2015).

From a functional point of view, the three RYR isoforms share several biophysical properties, including activation by submicromolar [Ca²⁺], calmodulin, ATP, and caffeine, as well as inhibition by micromolar [Mg²⁺], low and high calmodulin, ruthenium red, and procaine. They also share similar units of conductance (Ogawa et al., 2000). Nevertheless, there are important differences, such as RYR3's increased resistance to inactivation by high concentrations of Ca²⁺ (Ogawa et al., 2000). From a physiological point of view, RYR3s are not essential, as reflected by the fact that *ryr3*^{-/-} mice grow and reproduce

¹Department of Anesthesia, Basel University Hospital, Basel, Switzerland; ²Department of Biomedicine, Basel University Hospital, Basel, Switzerland; ³Department of Ophthalmology, University Hospital of Bern, Bern, Switzerland; ⁴Department of Biomedical Research, University of Bern, Bern, Switzerland; ⁵Department of Surgery, Davis Heart & Lung Research Institute, The Ohio State University Medical Center, Columbus, OH; ⁶Graduate School of Pharmaceutical Sciences, Kyoto University, Kyoto, Japan; ⁷Department of Life Sciences, Microbiology and Applied Pathology section, University of Ferrara, Ferrara, Italy.

*F. Zorzato and S. Treves contributed equally to this paper; Correspondence to Susan Treves: susan.treves@unibas.ch.

© 2019 Eckhardt et al. This article is distributed under the terms of an Attribution–Noncommercial–Share Alike–No Mirror Sites license for the first six months after the publication date (see <http://www.rupress.org/terms/>). After six months it is available under a Creative Commons License (Attribution–Noncommercial–Share Alike 4.0 International license, as described at <https://creativecommons.org/licenses/by-nc-sa/4.0/>).

normally and do not exhibit gross abnormalities in smooth muscle cell function (Takeshima et al., 1996). However, developing skeletal muscles from *ryr3*^{-/-} mice exhibit reduced twitch amplitudes in response to electrical stimulation and caffeine addition, but the lack of RYR3 does not apparently impact the function of adult muscles (Bertocchini et al., 1997). Interestingly, *ryr3*^{-/-} mice exhibit behavioral abnormalities, including increased locomotor activity, impaired performance in the water maze, and a mild tendency to circular running (Balschun et al., 1999).

Extraocular muscles (EOMs) are classified as a distinct muscle allototype when compared with limb and dorsal muscles. They are either selectively spared in certain congenital muscle diseases such as Duchenne muscular dystrophy or preferentially affected in conditions such as myasthenia gravis and mitochondrial myopathies, indicating that they are biochemically different from their limb muscle counterpart. EOMs have a unique embryonic origin, can be singly or multiply innervated, contain a large number of mitochondria, are highly vascularized, do not store glycogen, are fatigue resistant, and express distinct myosin heavy chain (MyHC) isoforms (Spencer and Porter, 1988; Hoh et al., 1989; Kaminski and Ruff, 1997; Porter et al., 2001; Ketterer et al., 2010; Zhou et al., 2010). Furthermore, they contain a population of preactivated satellite cells that continuously fuse into existing myofibers under “uninjured” conditions (McLoon and Wirtschafter, 2002a,b; Stuelsatz et al., 2015).

While investigating the biochemical and physiological characteristics of human EOMs, we reported that such muscles contain a distinct toolkit component of the proteins involved in ECC, as they express both Ca_v1.1 and Ca_v1.2 (the skeletal and cardiac isoform of the α 1 subunit of the DHPR, respectively), calsequestrin 1 and 2, RYR1, and RYR3, resulting in distinct intracellular calcium homeostasis properties (Sekulic-Jablanovic et al., 2015). In the present study, we used the *ryr3*^{-/-} mouse model to investigate the function of RYR3 in EOMs. Our data show that constitutive ablation of RYR3 significantly affects both the mechanical properties of mature EOMs and calcium homeostasis, and we propose that these changes are responsible for the impaired visual functions of *ryr3*^{-/-} mice.

Materials and methods

Animal model and ethical permits

The *ryr3*^{-/-} mouse model was generated by Takeshima et al. (1996). Experiments were performed on 8–12-wk-old mice. All experimental procedures were approved by the Cantonal Veterinary Authorities (BS Kantonales Veterinärämamt permit numbers 1728 and 2115 and BE Kantonales Veterinärämamt BE32/15). All experiments were performed in accordance with relevant guidelines and regulations.

Assessment of visual acuity by the Morris water maze task

Visual acuity was tested using the cued Morris water maze (Enzmann et al., 2006; Zulliger et al., 2011). A round gray tank of 1.7-m diameter filled to a height of 30 cm with water at room temperature (23 ± 1°C) was used. The water was made opaque by

the addition of nontoxic white paint. A video camera fastened above the center of the pool recorded the swimming pattern of the mice using a video tracking system (Ethovision XT11; Noldus Information Technology). The water surface was virtually divided into four quadrants, and there were four entry zones to the pool. A white, round platform with a diameter of 20 cm was placed in one quadrant at a distance of 50 cm from the border and 1.5 cm above the water surface. Four entry zones were marked outside the pool. The room was illuminated at an intensity of <150 Lux. Animals were transferred to the experimental room 72 h before the experiments in order to acclimatize them. The light in the room was switched on at 6 a.m., and the mice were exposed to 12-h light/dark cycles. Mice were provided with water and food ad libitum. On day 0, mice performed a habituation run, swimming for 60 s in the water maze. On day 1, mice performed four trials with the platform at a fixed position and varying each of the four entry zones; the test duration was 60 s per run. If the mice did not find the platform after 60 s, then they were guided to it by hand and allowed to stay on it for 10 s. On day 2, the tests were repeated similarly to day 1, except that the platform was moved in the opposite quadrant. The following parameters were evaluated: swimming velocity, total distance moved, and time to reach the platform. The results are presented as average per experimental group, per day. Heat maps showing the relative combined traces of the mice for each group were generated using Ethovision.

Optokinetic reflex (OKR)

The OptoMotry System from CerebralMechanics was used to measure the OKR as previously described (Prusky et al., 2004; Thomas et al., 2004). Briefly, a virtual cylinder comprising a vertical sine wave grating was projected in 3-D coordinate space on computer monitors (17" LCD computer monitors, model 1703FP; Dell) arranged in a square around and projecting to the testing area, consisting of a platform positioned 13 cm above a mirrored floor under a likewise mirrored lid. To record the behavior of the mice, a video camera (DCR-HC26; Sony) was positioned directly above the platform and connected to a computer, allowing live video feedback. The computer was also used to project the virtual cylinder on the monitors in a 3-D coordinated space, controlling the speed of rotation and geometry of the cylinder and spatial frequency of the stimuli. The image on the monitors was expanded by the mirrors on the floor and the ceiling, thereby creating a virtual 3-D world. To measure under scotopic conditions, light levels were attenuated with cylindrical neutral density filters (R211 0.9ND; LEE Filters) inside the tracking area, thereby reducing the ambient light in the testing area to a luminance level of -4.5 log cd m⁻².

During testing, the mice stood unrestrained on the platform tracking the 3-D pattern with a reflexive head movement. The movements of the mice on the platform were followed by the experimenter with a crosshair superimposed on the video image to center the rotation of the virtual cylinder with the x-y positional coordinates of the crosshair at the mouse's viewing position, maintaining the pattern at a constant distance from the animal. Mice normally stopped moving when a grating perceptible to them was projected onto the cylinder wall and the

cylinder was rotated and began tracking the pattern with reflexive head movements in concert with the rotation. The decision of whether the mouse tracked the pattern or not was made by the experimenter based on evident head movement against the stationary arm of the crosshair. Animals that slipped or jumped off the platform during the test trial were returned to the platform, and testing was continued. The measurements were always made in the morning, and all animals were acclimated to the testing by placing them on the platform for a few minutes without testing. Two independent experimenters were blinded both to the genotype and to previous records.

Electroretinography

Mice were dark-adapted overnight. The animals were then anesthetized using 80 mg/kg ketamine (Ketalar 50 mg/ml; Pfizer AG) and 1 mg/kg medetomidine (Domitor; Orion Pharma). Pupils were dilated at the time of anesthesia by topical instillation of 2.5% phenylephrine + 0.5% tropocamide (MIX-Augentropfen; ISPI), and oxybuprocaine (Oxybuprocaine 0.4% SDU Faure; Thea Pharma) was used for additional local anesthesia. The anesthetized mice were positioned in the recording apparatus (Ganzfeld stimulator Q400; Roland Consult). The scotopic electroretinogram was elicited at different light intensities (-25, -20, -10, 0, +10, and +15 dB). Eight flashes (256-ms duration) were presented at 0.1 Hz with a 20-ms interval, and the responses were averaged. A- and B-wave amplitudes were quantified using the RETI-port/scan 21 analysis tool (Roland Consult). The anesthesia was revoked by injection of 2.5 mg/kg atipamezole (Antisedan; Orion Pharma), but never before 30 min after initiation of the anesthesia.

Isometric force measurements

Isolated EOMs were mounted intact on a MyoStation (Myotronic). The force transducer was equipped with small hooks. One of the rectus muscles, mainly medial, was tied with a prolene suture (EP8703H; Ethicon) by stitching through the eyeball close to the entry point of the muscle. The other side was ligated on the left over the orbital socket bone with a surgical suture (SP102; Look). After ligation, the remaining EOMs, the optic nerve, and the retractor bulbi muscle were surgically removed. For the force measurements, EOMs were stimulated with a single pulse of 0.5 ms and of 24.6 V. Experiments were performed at 30°C. Muscle force was digitized at 4 kHz using an ADInstruments. Results were analyzed using the principal-component analyses (Hwang et al., 2013) included in the OriginPro 2017 (OriginLab Corp) software package.

Quantitative real-time PCR

Total RNA was extracted from the EOMs using Trizol (15596-018; Invitrogen) following the manufacturer's protocol. After treatment of the RNA with deoxyribonuclease I (18068-015; Invitrogen), 1,000 ng was reverse transcribed using the high-capacity complementary DNA (cDNA) Reverse Transcription kit (4368814; Applied Biosystems). cDNA was amplified by quantitative real-time PCR using Power Sybr Green Master Mix (4367659; Applied Biosystems) as previously described (Sekulic-Jablanovic et al., 2015, 2016). The sequence of

the primers used for quantitative PCR (qPCR) is given in Table S1. qPCR was performed on a 7500 Fast Real-Time PCR machine from Applied Biosystems using 7500 software v2.3. Gene expression was normalized to expression ACTN2, which is present in all muscle fiber types. Results are expressed as fold change of gene expression in *ryr3*^{-/-} mice compared with its expression in WT mice, except for when the values of RYR1 and RYR3 were compared in EOMs from WT mice, in which case the value of RYR3 was set to 1.

Electrophoresis and immunoblotting

Total muscle homogenates were prepared from flash-frozen EOM samples in 10 mM HEPES, pH 7.0, 150 mM NaCl, 1 mM EDTA, and anti-protease (11873580001; Roche) as previously described (Sekulic-Jablanovic et al., 2015, 2016). Protein concentration was determined using a Protein Assay Kit II (5000002; Bio-Rad Laboratories), and BSA was used as a standard. SDS-PAGE, protein transfer on to nitrocellulose membranes, and immunostaining were performed as previously described (Sekulic-Jablanovic et al., 2015), except for parvalbumin. In the latter case proteins were separated on a 10% Tris-Tricine gel (Schägger and von Jagow, 1987) and subsequently transferred onto nitrocellulose. The following primary antibodies were used for Western blotting: rabbit anti-RYR1 (8153S; Cell Signaling), goat anti-Ca_v1.1 (sc-8160; Santa Cruz), rabbit anti-Ca_v1.2 (sc-25686; Santa Cruz) rabbit anti-calsequestrin-1 (C-0743; Sigma) and calsequestrin-2 (ab-3516; Abcam), goat anti-SERCA1 (sc-8093; Santa Cruz), goat anti-SERCA2 (sc-8095; Santa Cruz), mouse anti-MyHC (05-716; Millipore), mouse anti-MyHC13 (4A6; DSHB Iowa), rabbit anti-Desmin (sc-14026; Santa Cruz) and rabbit anti-parvalbumin (PV25; Swant), and rabbit anti-JP-45 (Zorzato et al., 2000). Secondary peroxidase conjugates were Protein G-peroxidase (P8170; Life Technologies) and peroxidase-conjugated goat anti-mouse IgG (A2304; Sigma). The immunopositive bands were visualized by chemiluminescence using the WesternBright ECL-HRP Substrate (K-12045-D50; Advansta) or the Chemiluminescence kit from Roche (11500694001; Roche) on a Vilber Fusion Solo S system. Statistical analysis of the intensity of the immunopositive bands was determined using ImageJ/FIJI (Schindelin et al., 2012). The intensity values were normalized to the intensity of the indicated skeletal muscle-specific protein.

Single-fiber isolation

Mice were sacrificed with a Pentobarbital overdose, their hearts were cannulated, and the circulatory system was washed with mammalian Ringer buffer (137 mM NaCl, 5.4 mM KCl, 1 mM MgCl₂, 0.1% glucose, and 11.8 mM HEPES, pH 7.4). Subsequently, 17 ml of a collagenase cocktail prepared in modified mammalian Ringer buffer (137 mM NaCl, 5.4 mM KCl, 0.5 mM MgCl₂, 1.8 mM CaCl₂, 0.1% glucose, and 11.8 mM HEPES, pH 7.4) containing 20 mg collagenase type I (*Clostridium histolyticum* type I, C0130; Sigma), 6 mg collagenase type 2 (LS004176; Worthington Biochemical Corporation), and 2.5 mg Elastase (LS002294; Worthington Biochemical Corporation) was injected into the circulatory system. EOMs were removed under a dissecting microscope and further digested in a small Erlenmeyer flask

containing 0.2% collagenase type 2 and 0.1% Elastase, in mammalian Ringer for 70 min at 37°C, 5% CO₂. At the end of the digestion, fibers were gently separated from the tendons by passing them through progressively narrower pipette tips.

Immunofluorescence

Isolated EOM fibers were pipetted onto laminin and collagen-coated Ibidi μ -Slide 4 well or μ -Slide 8 well chambers (#80426 and #80826). The fixation and permeabilization steps depended on the antibody being used. For Ca_v1.1 and Ca_v1.2, 4% paraformaldehyde (made in PBS) was used as a fixative and 1% Triton in PBS for permeabilization and processed as previously described (Treves et al., 2011). For RYR1 and Ca_v1.1 staining, fibers were fixed in ice-cold (-20°C) methanol for 15–30 min and permeabilized in 2% Triton in PBS for 20–30 min. After staining with the appropriate secondary antibodies, the fibers were incubated with 4',6-diamidino-2-phenylindole (DAPI) to visualize the nuclei. The following primary and secondary antibodies were used: rabbit monoclonal anti-RYR1 (D4E1, #8153; Cell Signaling), mouse monoclonal anti-Ca_v1.1 (IIC12D4 and IIID5E1; Iowa Hybridoma bank), rabbit anti-Ca_v1.2 (sc-25686; Santa Cruz), Alexa Fluor 568 donkey anti-mouse IgG (A10037; Invitrogen), and Alexa Fluor 488 chicken anti-rabbit IgG (A21441; Invitrogen). A Nikon A1R confocal microscope with a 60 \times oil-immersion Plan Apo VC Nikon objective (numerical aperture, 1.4) was used to make the images (Lopez et al., 2016).

Single-fiber calcium measurements

All measurements were performed at room temperature. The resting Ca²⁺ fluorescence in single fibers was measured on glass-bottom culture dishes (P35G-0-14-C; MatTek) using the ratiometric calcium indicator fura-2 AM (F1201; Invitrogen; Treves et al., 2011; Sekulic-Jablanovic et al., 2015, 2016). For electrically evoked Ca²⁺ transients, isolated EOM fibers were allowed to settle on laminin (L2020; Sigma) and collagen-coated μ -Slide 4 well from Ibidi. Fibers were incubated for 20 min at 20°C in Ringer's solution containing 10 μ M of the low-affinity calcium indicator Mag-Fluo-4 AM (M14206; Invitrogen; Hollingworth et al., 2009). Custom-designed 3-D-printed electrodes were used to stimulate the fibers with a 0.5-ms bipolar pulse using a computer-controlled stimulator (MyoDat+ Stimulator Amplifier; Myotronic). A Nikon A1R laser-scanning confocal microscope (Nikon Instruments) with a 60 \times oil-immersion Plan Apo VC Nikon objective (numerical aperture, 1.4) in resonant mode at super-high temporal resolution (7,918 fps) was used to record the linescans. For spark measurements, fibers were loaded with 5 μ M Fluo-4 (F14217; Invitrogen), and experiments were performed as previously described (Lopez et al., 2016).

Myotube isolation and calcium measurements

Isolated EOMs were minced into small fragments. Satellite cells contained within the fragments were allowed to grow on laminin-coated glass bottom culture dishes (P35G-0-14-C; MatTek Corporation) in growth medium (DMEM plus 4.5 mg/ml glucose, 10% horse serum, 5 ng/ml insulin, 200 mM glutamine,

600 ng/ml penicillin G and streptomycin, and 7 mM HEPES, pH 7.4), and once a sufficient number of myoblasts had grown, the culture medium was switched to differentiation medium (DMEM plus 4.5 mg/ml glucose, 0.5% BSA, 10 ng/ml epidermal growth factor, 0.15 mg/ml creatine, 5 ng/ml insulin, 200 mM glutamine, 600 ng/ml penicillin G and streptomycin, and 7 mM HEPES, pH 7.4) to obtain myotubes, as previously described (Sekulic-Jablanovic et al., 2015). The resting calcium concentration and the total amount of rapidly releasable Ca²⁺ stores were measured using the ratiometric calcium indicator fura-2 AM as previously described (Sekulic-Jablanovic et al., 2015, 2016). For measurements of myotube calcium oscillations and sparks, cells were loaded with 5 μ M Fluo-4 as previously described (Sekulic-Jablanovic et al., 2015, 2016) and experiments were performed at room temperature.

Analysis of calcium transients

Linescans were saved as stacked images using the microscope software (NIS-Elements, version 4.60). A plug-in for Icy (de Chaumont et al., 2012) was written to concatenate the linescans and calculate their profiles in one step. The plugin has the possibility of adding regions of interest and performing calculations on the regions of interest. For analysis of the peak Ca²⁺ and Ca²⁺ kinetics in fibers and myotubes a Ca²⁺ analysis program in Microsoft's .net Framework (<https://visualstudio.microsoft.com>) was designed. The analysis of the Ca²⁺ peaks for fibers and myotubes is similar but not identical; the fiber profile files contain only one transient, and the program requires information only on the number of header columns contained within the file. The myotube profiles are larger since they contain multiple transients. Therefore, the program requires an additional file (Peak-Summary) to analyze their profiles, containing, among other information, data relative to the beginning, the end, and the location of the maximum value of each peak within the profile. The Peak-Summary files were created in OriginPro 2018 by a batch peak search of the raw data.

For analysis of the Ca²⁺ transient, the baseline was calculated as the average of the first 5 ms of the profile. Once the maximum height of the transient was reached, the $\Delta F/F$ was calculated. The beginning of the peak was defined as the time where the transient increased by 5% of the maximum height, with respect to the baseline, for the first time. Time to peak (TTP) is the time from the beginning of the peak to the maximum height. Time to half peak (TTHP) is the time from the beginning of the peak to the time where the transient increases by 50% of the maximum height with respect to the baseline for the first time. Half relaxation time (HRT) is the time from the maximum height until the time where the transient is higher than 50% of the maximum height, for the last time. These parameters were calculated by the Ca²⁺ analysis program. For an automated kinetic analysis of the fiber transient, a Savitzky–Golay smoothing with polynomial order of 2 and window size of 12 was applied, while the $\Delta F/F$ calculations were done on the raw data. Savitzky–Golay smoothing is known for preserving the area, position, and width of peaks better than a moving average filter (Guiñón et al., 2007; Ostertagova and Ostertag, 2016).

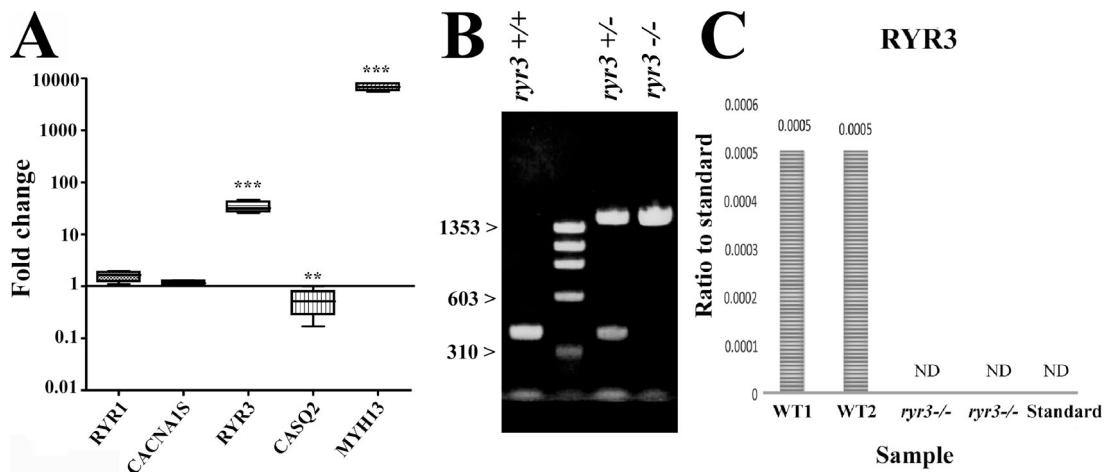


Figure 1. **RYR3 is expressed in murine EOM.** (A) Expression of ECC transcripts in mouse EOM muscles. Transcript levels were quantified by qPCR in muscles from three WT mice (performed twice in triplicate). Values are plotted as mean (SEM) change in EOM vs. hindlimb muscles, which was set as 1. **, $P < 0.01$; ***, $P < 0.001$, Student's t test. Primers used are detailed in Table S1. (B) Genotyping WT and $ryr3^{-/-}$ mice using the primers detailed in Table S1; PCR amplification of genomic DNA from the $ryr3^{-/-}$ mouse yields a DNA fragment that is $>1,000$ bp larger than that of WT mice, compatible with the insertion of a $>1,000$ -bp cassette in exon 1. Amplification of genomic DNA from heterozygous mice shows the presence of the smaller WT allele and the larger allele containing the inserted cassette. (C) Mass spectrometry analysis of EOMs from two WT and two $ryr3^{-/-}$ mice shows the absence of RYR3. ND, not detectable.

Statistical analysis and graphical software

Statistical analysis was performed using the unpaired two-tailed t test for equal variance and the unpaired two-tailed Welch's t test for unequal variance and unequal sample size. Means were considered statistically significant when the P value was <0.05 . Data were processed, analyzed and plotted using the software OriginPro 2018 (OriginLab Corporation). Images were assembled using Adobe Photoshop CS (version 8.0).

Online supplemental material

Fig. S1 shows that retinal morphology and layer structure is unaltered in $ryr3^{-/-}$ mice. Fig. S2 shows photomicrographs of myotubes from EOM. Table S1 lists primers used for qPCR and for mouse genotyping. Table S2 lists kinetic properties of isolated EOM from WT and $ryr3^{-/-}$ mice. Video 1 shows a WT mouse swimming in a cued water maze. Video 2 shows a $ryr3^{-/-}$ mouse swimming in a cued water maze.

Results

$ryr3^{-/-}$ mice have a defect in their visual acuity, and isolated muscles exhibit altered kinetic parameters

Mouse EOMs are similar to their human counterpart in that they express high levels of RYR3 compared with limb muscles (Fig. 1 A); the ratio of RYR1 to RYR3 in WT mouse EOMs was assessed by qPCR and found to be 323 ± 65 to 1 (mean \pm SEM, $n = 4$). We used $ryr3^{-/-}$ transgenic mice to evaluate the function of RYR3 in eye muscles. The total body $ryr3^{-/-}$ mouse line used in the present investigation was created by conventional gene targeting and was previously characterized by Takeshima et al. (1996). The presence of a cassette of $\sim 1,000$ bp disrupting exon 1 of the genomic RYR3 DNA was confirmed by PCR amplification (Fig. 1 B), and the absence of RYR3 protein was confirmed by mass spectrometry analysis (Fig. 1 C).

To assess visual function in WT and $ryr3^{-/-}$ mice, we used complementary noninvasive parameters, namely the cued water maze and the OKR test (Prusky et al., 2004; Thomas et al., 2004; Zulliger et al., 2011). The Morris water maze is a standard method used to assess spatial learning in rodents (Thomas et al., 2004; Zulliger et al., 2011). In one of its versions, animals need to locate a visible platform and are subsequently scored according to the total swimming distance and time required to identify the platform. Thereby, the animal relies on visual information to locate a platform. This test is often used to control for visual ability (Brown and Wong, 2007). As shown in Fig. 2 A and Videos 1 and 2, $ryr3^{-/-}$ mice performed significantly worse than age-matched WT mice. In particular, the mean swimming distance necessary to find the platform was increased by $\sim 50\%$, and the mean time taken to find the platform was increased by $\sim 30\%$ (Fig. 2 A). Qualitatively similar results were obtained when visual acuity was assessed using the OptoMotry detection system, a simple and precise method for quantifying mouse vision (Prusky et al., 2004). It assesses the OKR, an involuntary fixation on objects that are moving in relationship to the head. The eyes have the tendency to track moving objects for a distance and then subsequently saccade in the opposite direction to reacquire a target. Saccades rely on EOMs to move the eyes the correct distance in the appropriate direction (Purves et al., 2001). In the OptoMotry detection system, unrestrained mice are placed on a central platform inside a virtual 3-D cylinder, and the reflective head movements in response to changes in the spatial frequency movement of a grid are scored (Thomas et al., 2004). The top panel of Fig. 2 B shows a schematic representation of the test setup (reproduced with permission from Prusky et al., 2004), and the bottom panel shows the results obtained in individual male and female mice. As shown in the figure, the visual acuity of $ryr3^{-/-}$ mice was decreased by $\sim 20\%$ compared with WT mice. The

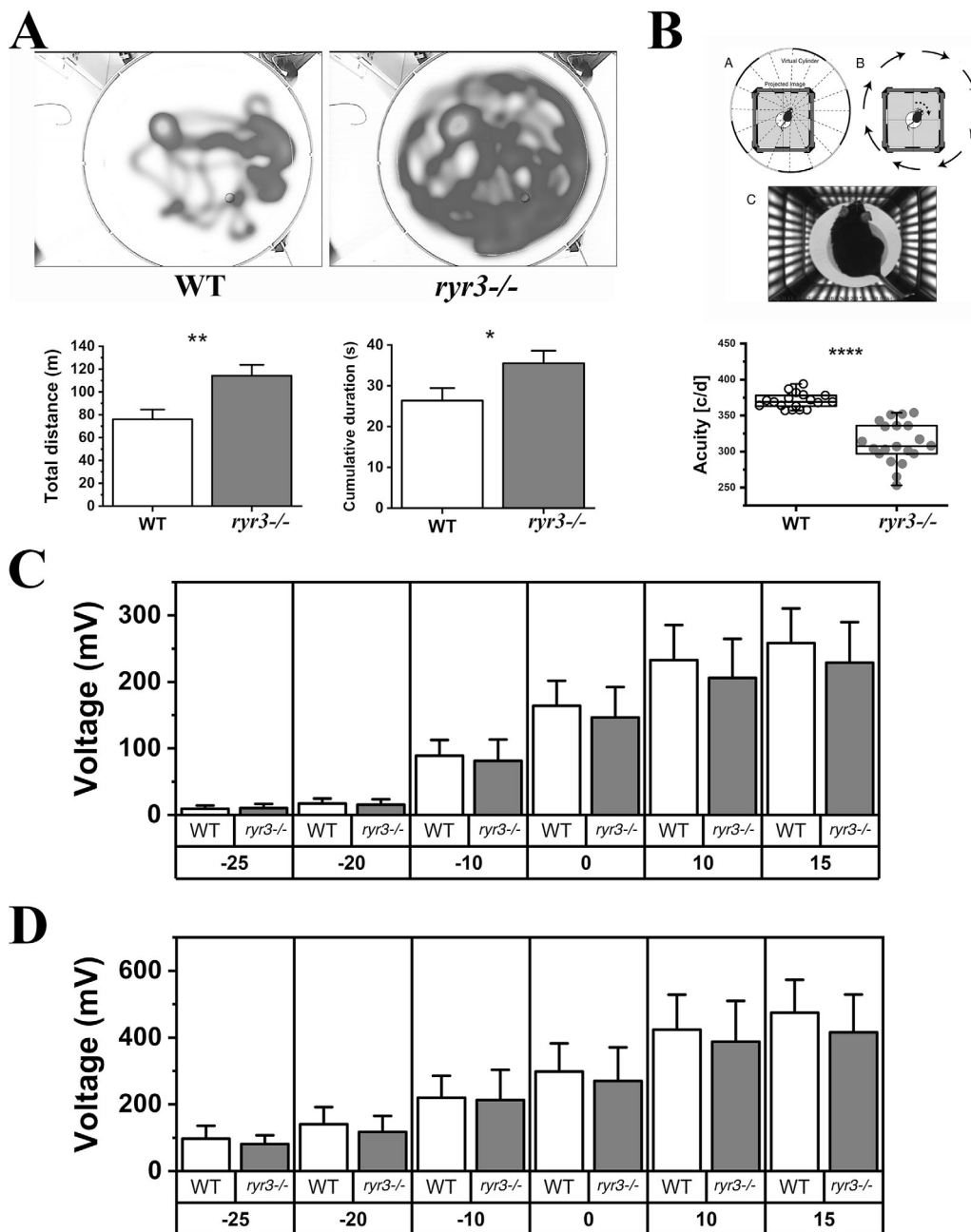


Figure 2. ***ryr3*^{-/-} mice exhibit visual impairment.** (A) Cued water maze. Top: Representative heatmaps of the swimming path of WT (left) and *ryr3*^{-/-} (right) mice. Bottom left: Total swimming distance (mean ± SEM) required to reach the platform. Bottom right: Time required to reach the platform. Experiments were performed on 10 mice per strain, and data from four different pool entry points were combined. (B) OKR. Top: OptoMotry setup. From Prusky et al. (2004), Fig. 2 B is reprinted with permission from *Investigative Ophthalmology & Visual Science*. Bottom: Visual acuity of two independent measurements performed under scotopic conditions on each mouse. Each symbol represents the visual acuity of a single mouse; empty circles, WT mice (n = 20); gray circles, *ryr3*^{-/-} mice (n = 20). The unit of visual acuity is cycles/degree (c/d). (C and D) Scotopic ERG results of n = 9 WT (empty boxes) and n = 10 *ryr3*^{-/-} (gray boxes). Amplitude (in millivolts) of A-waves (C) and B-waves (D); the x axes represent the intensity of the illuminating flash. *, P < 0.05; **, P < 0.005; ****, P < 0.0001, Student's t test.

results shown in Fig. 2 were obtained by pooling male and female mice, which were similar in their response. The decrease in visual capacity of *ryr3*^{-/-} mice was not caused by alterations of the retinal function, since the electroretinogram under scotopic conditions was similar in WT and *ryr3*^{-/-} mice (Fig. 2, C and D). The decrease in visual capacity was also not caused by alterations in the structure of the retina as a

consequence of RYR3 ablation, since no changes were observed in retinal thickness, spatial distribution, and appearance of the different layers constituting the retina (Fig. S1). Taken together, these results show that in vivo, *ryr3*^{-/-} mice have an alteration of their visual capacity, but they do not discriminate whether the problem is of neuronal origin or relates to skeletal muscle function.

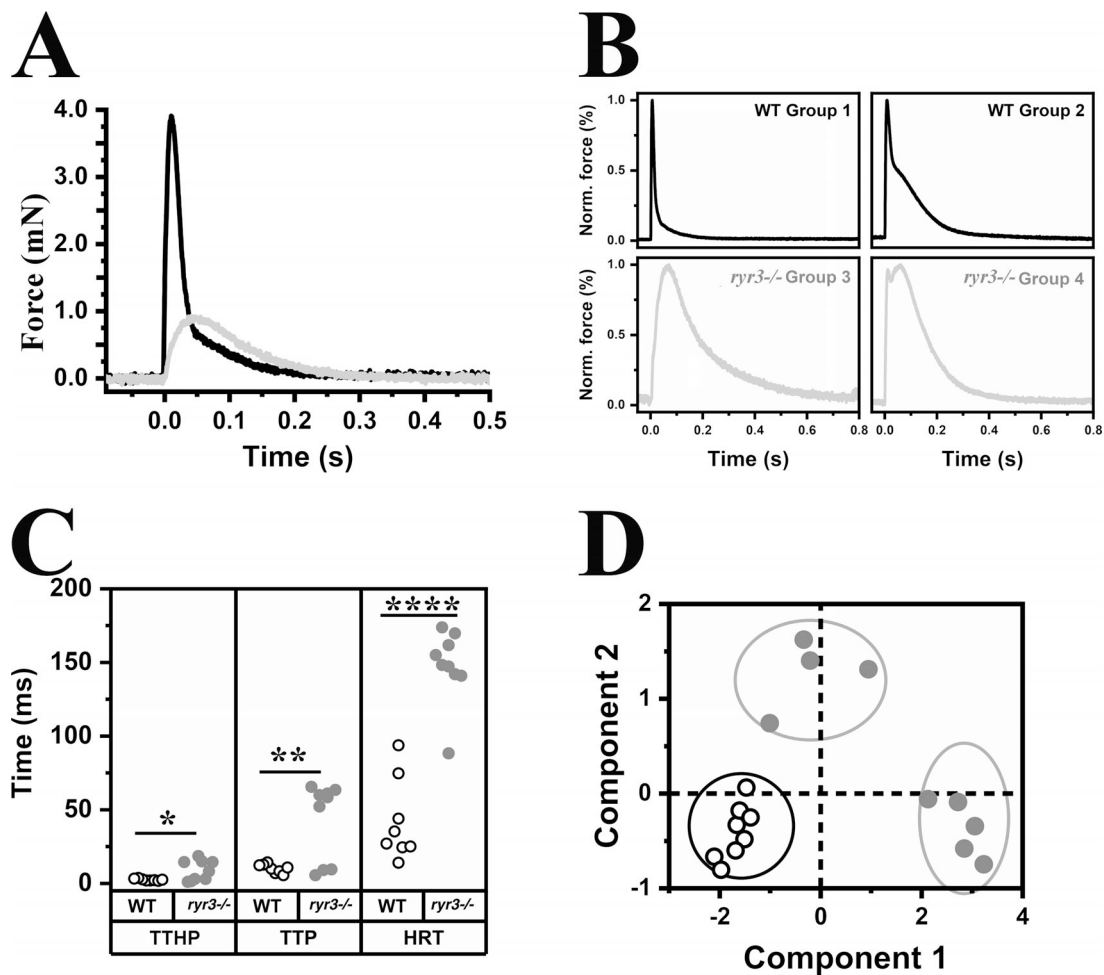


Figure 3. Ex vivo isometric force measurements in mouse EOMs. (A) Representative trace of the absolute twitch force obtained from isolated single extraocular rectus muscles from WT (black line; $n = 8$) and $ryr3^{-/-}$ (gray line; $n = 9$) muscles. Muscles were stimulated by electric field stimulation with a pulse of 24.6 V having a duration of 0.5 ms. (B) Objective classification of force measurements into four groups. The force was normalized to the maximum of each transient to illustrate the differences in the kinetics as well as the presence or absence of the fast and slow component of the twitch. (C) Kinetic twitch parameters (TTHP, TTP, and HRT). Each symbol represents the kinetic parameters of a single rectus EOM from a single mouse; empty circles, WT mice; gray circles, $ryr3^{-/-}$ mice. *, $P < 0.05$; **, $P < 0.001$; ****, $P < 0.0001$, Student's t test. Experiments were performed at room temperature. (D) Principal-component analyses of five twitch parameters (slow amplitude, fast amplitude, TTHP, TTP, and HRT). The axes represent the two principal components.

To answer this question directly, we investigated the mechanical properties of isolated EOM using a MyoStation-intact force transducer modified to measure twitch force in mounts of mouse EOMs as detailed in Materials and methods. In the experimental setup, we removed the oblique muscles and measured the force generated by electrical stimulation of medial rectal muscles. The force generated in response to a single pulse of 0.5 ms and of 24.6 V was significantly reduced and slower in EOMs from $ryr3^{-/-}$ mice (Fig. 3, A and B, light gray line; Table S2). The maximal peak force developed was $\sim 38\%$ of that developed by EOMs from WT mice (WT: 0.328 ± 0.095 mN, $n = 8$; $ryr3^{-/-}$: 0.126 ± 0.017 mN, $n = 9$; Fig. 3, A and B, black line), and the kinetics was significantly slower. The kinetic properties of the muscles were not uniform and could be classified into four groups: twitches with a single rapid peak and rapid relaxation time (WT group 1), a rapid peak and a two-phased relaxation time of which one was rapid and the other slower (WT group 2), a slow peak and a slow relaxation time ($ryr3^{-/-}$ group 3), and

rapid twitch with a double peak and slow relaxation time ($ryr3^{-/-}$ group 4). To facilitate their direct comparison, the individual peak maximal forces were each set to 100%. The results plotted in Fig. 3 C and detailed in Table S2 show that there were significant differences in the kinetic properties of WT and $ryr3^{-/-}$ EOMs. The mean TTHP was 2.5 ± 0.2 and 8.8 ± 2.3 ms, the mean TTP was 10.1 ± 1.1 and 42.8 ± 8.8 ms, and the mean HRT was 42.3 ± 9.8 and 147.4 ± 8.4 ms in WT ($n = 8$) and $ryr3^{-/-}$ mice ($n = 9$), respectively (values are the mean \pm SEM). Fig. 3 D shows the kinetic data analyzed according to the principal-component analyses. This statistical procedure allows the simultaneous comparison of multiple variables or parameters that are reduced to a smaller set of data, facilitating the comparison of data by grouping similar datasets (Hwang et al., 2013). Analysis of the twitch parameters of muscles from WT mice (empty dots, Fig. 3 D) indicates that the values are similar to each other and can all be grouped into one cluster (bottom left, black bordered circle, Fig. 3 D); on the other hand, the data from the $ryr3^{-/-}$

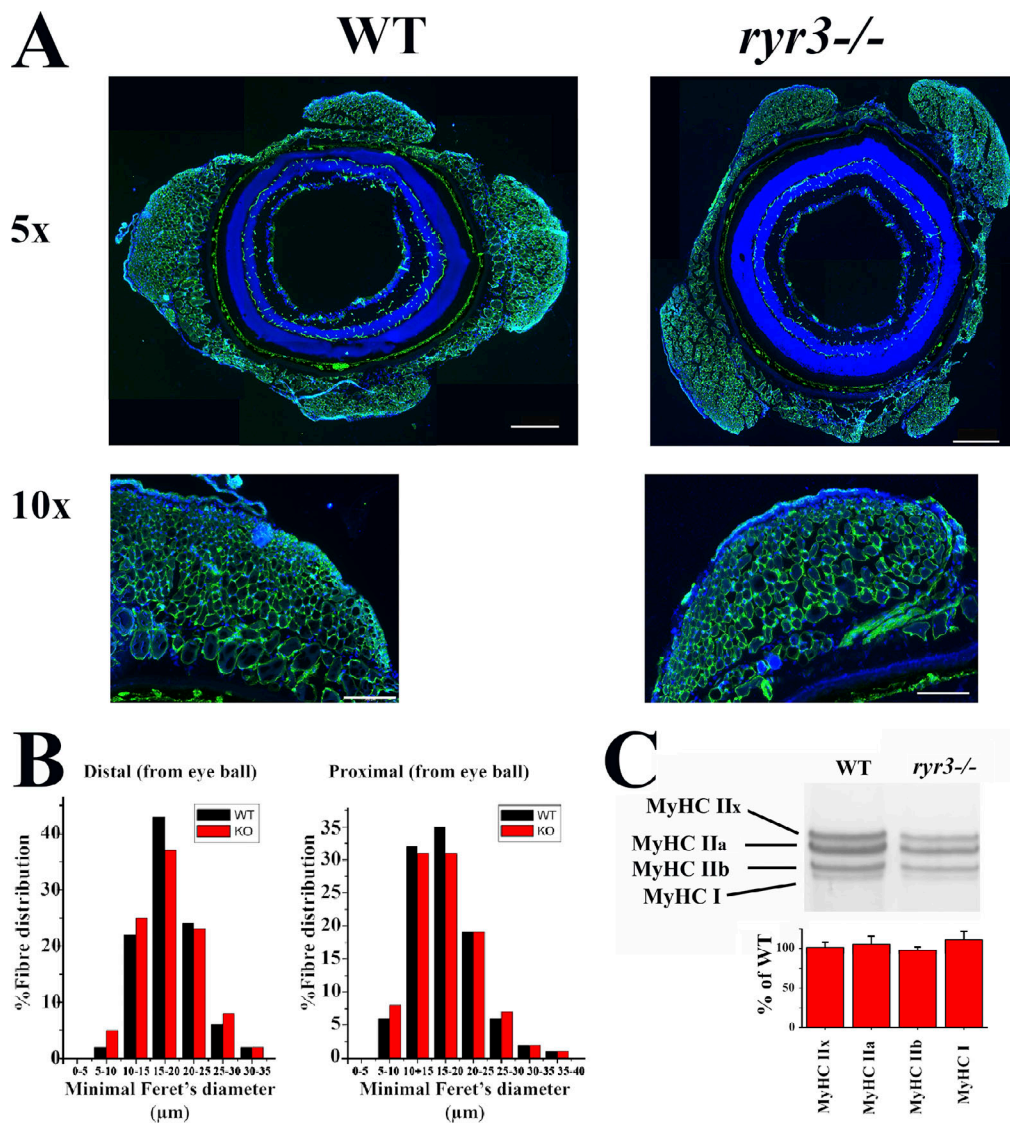


Figure 4. **Fiber type distribution and MyHC composition is similar in EOM muscles from WT and *ryr3*^{-/-} mice.** (A) EOM from WT and *ryr3*^{-/-} mice were sectioned, stained with anti-MyHC recognizing all isoforms and DAPI, and observed by fluorescent microscopy. Scale bars represent 500 μm (5× images) and 200 μm (10× images). (B) The fiber size distribution of EOMs was determined using the minimal Feret's diameter using MyHC immunohistochemistry (Delbono et al., 2007; black bars, WT; red bars *ryr3*^{-/-}). (C) High-resolution SDS-PAGE separation of MyHC isoforms in WT and *ryr3*^{-/-} EOM muscles (Talmadge and Roy, 1993). The bottom bar graphs show the percent specific MyHC isoform vs. total MyHC content in *ryr3*^{-/-} relative to WT (mean ± SEM, *n* = 5 WT and *n* = 5 *ryr3*^{-/-}), which was set to 100%.

muscles (gray dots, Fig. 3 D) fall not within the same cluster but within two completely separate clusters (gray bordered circles, Fig. 3 D). These changes in the mechanical properties were not caused by muscle atrophy, as the overall size distribution of fibers within the eye muscles (minimal Feret's diameter) was similar in WT and *ryr3*^{-/-} mice (Fig. 4, A and B), nor were the changes caused by gross alterations in the overall MyHC isoform composition (Fig. 4 C).

The content and subcellular localization of proteins involved in ECC in EOM from WT and *ryr3*^{-/-} mice are similar

The changes in visual acuity and mechanical properties of the EOM from *ryr3*^{-/-} mice could be due to alterations in the content of proteins involved in ECC and/or in their subcellular localization.

Analysis of the transcripts encoding the major proteins involved in calcium regulation revealed only small differences between WT and *ryr3*^{-/-} mice, with the latter mice showing a reduction in RYR1 and CASQ1 transcripts (Fig. 5 A). The expression levels of the Ca_v1.1 (CACNA1S) and Ca_v1.2 isoforms (CACNA1C) of the α 1 subunit of the DHPR were not affected by RYR3 ablation (Fig. 5 A). As to protein levels, quantitative Western blot analysis did not reveal significant changes in content of proteins involved in ECC, except for an increase in parvalbumin (Fig. 5, B and C). We tested all commercially available anti-RYR3 antibodies, but none appeared to be specific. The absence of the RYR3 protein was confirmed by mass spectrometry analysis (Fig. 1 C).

To verify whether the observed changes in the mechanical properties of isolated EOMs in *ryr3*^{-/-} mice were due to

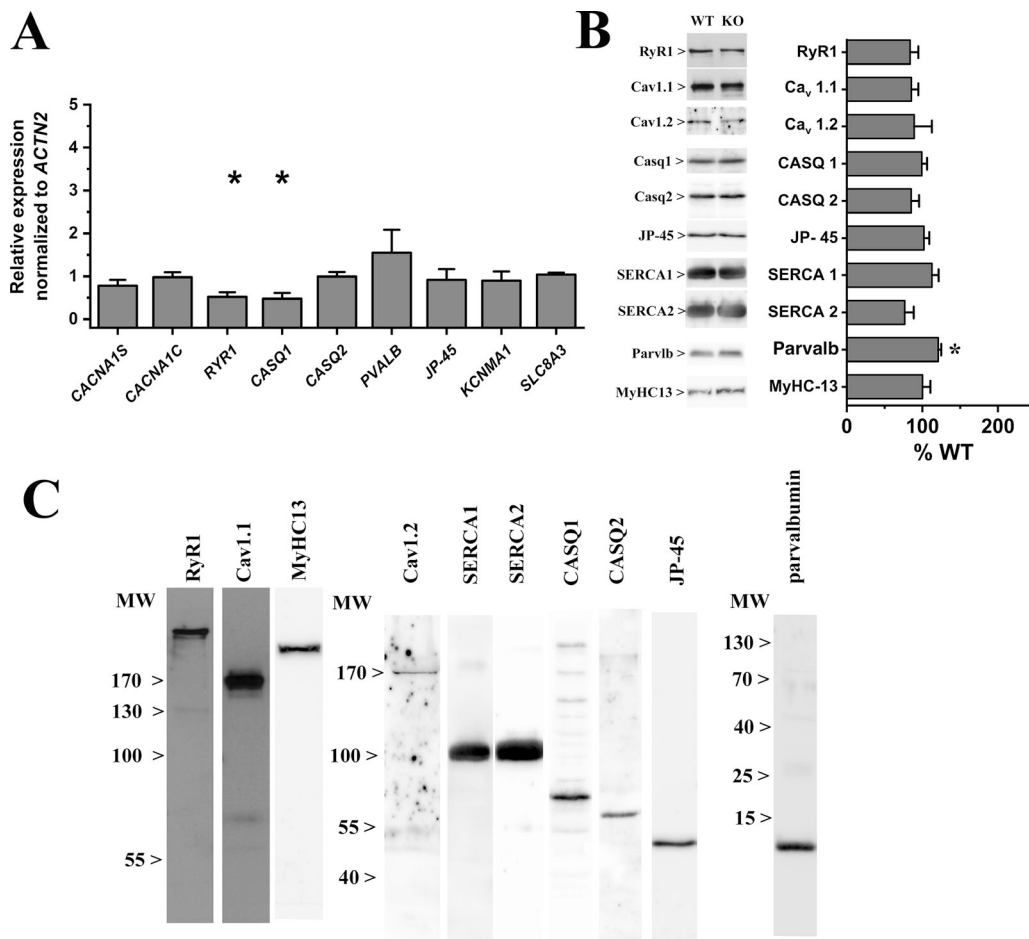


Figure 5. Transcript expression and protein content of key players involved in skeletal muscle calcium homeostasis. (A) Expression levels of transcripts encoding ECC proteins measured by qPCR. Values are plotted as mean (\pm SEM) fold change in *ryr3*^{-/-} vs. WT levels (which were set as 1). *ACTN2* was used as housekeeping gene. The mean expression level of duplicate determinations obtained from pooled EOM from four to six mice is shown. Transcript levels of *RYR1* and *CASQ1* were reduced by ~50%. *, $P < 0.05$, Student's *t* test. **(B)** Left: Representative immunopositive bands obtained from Western blots of EOM total homogenates probed with the indicated antibodies. Right: mean (\pm SEM) intensity values of the immunopositive bands normalized for desmin (except for MyHC13 that was normalized for total MyHC content). The mean intensity values were obtained from EOM muscles from four to eight mice. The intensity values of obtained from WT mice were set to 100%. *, $P < 0.05$, Student's *t* test. **(C)** The following commercial antibodies were used: rabbit anti-RyR1 (D4E1; 8153S; Cell Signaling), goat anti-Ca_v1.1 (sc-8160; Santa Cruz), rabbit anti-Ca_v1.2 (sc-25686; Santa Cruz), rabbit anti-calsequestrin-1 (CASQ1; C-0743; Sigma) and calsequestrin-2 (CASQ2; ab-3516; Abcam), goat anti-SERCA1 (sc-8093; Santa Cruz), goat anti-SERCA2 (sc-8095; Santa Cruz), mouse anti-MyHC (05-716; Millipore), mouse anti-MyHC13 (4A6; DSHB Iowa), and rabbit anti-parvalbumin (PV25; Swant). The rabbit anti-JP-45 polyclonal antibodies have been characterized previously (Zorzato et al., 2000). MW, molecular weight.

alterations in the subcellular localization of RYRs and/or of DHPs, high-resolution confocal immunohistochemistry was performed on enzymatically dissociated EOM fibers stained with different antibody combinations. Fig. 6 shows a representative image of fibers from WT and *ryr3*^{-/-} EOM stained for RYR1 (with rabbit anti-RYR1 mAb D4E1, whose epitope surrounds Arg830 of the human RYR1 protein; left panel, green color on the merged image) and of Ca_v1.1 (central panel, red color on merged images). The immunostaining of RYR1 and Ca_v1.1 was overall similar, as fibers from both mice showed the typical double row of overlapping fluorescence. More detailed analysis, however, revealed that the overlap of RYR1 and Ca_v1.1 fluorescence was reduced in fibers from *ryr3*^{-/-} (Table 1), indicating that RYR3 ablation affects the subcellular distribution of the RYR1 and Ca_v1.1 calcium channels. Fig. 6 B shows that Ca_v1.1 (mouse mAb, left panel, red fluorescence on merged image) and Ca_v1.2 (rabbit polyclonal Ab,

central panel, green fluorescence on merged image) do not share subcellular localization in EOMs. In fact, the fluorescent pattern of Ca_v1.2 showed a predominantly patchy appearance on the plasmalemma of the fibers, with low levels of fluorescence within the double rows that are positive for Ca_v1.1. The Ca_v1.2 antibodies are specific as they recognize a band of ~170 kD on Western blot (Fig. 5 C) and do not recognize any structure when tested on extensor digitorum longus (EDL) muscle fibers that lack the Ca_v1.2 isoform (Fig. 6 B, bottom central panel). There was no apparent difference in the subcellular localization of Ca_v1.2 between WT and *ryr3*^{-/-} mice (Table 1).

ECC in single EOM-muscle fibers and EOM-derived myotubes

Ca²⁺ homeostasis and the ECC characteristics of fibers isolated from WT and *ryr3*^{-/-} mice were analyzed by fluorescence microscopy. Enzymatically dissociated fibers were loaded either

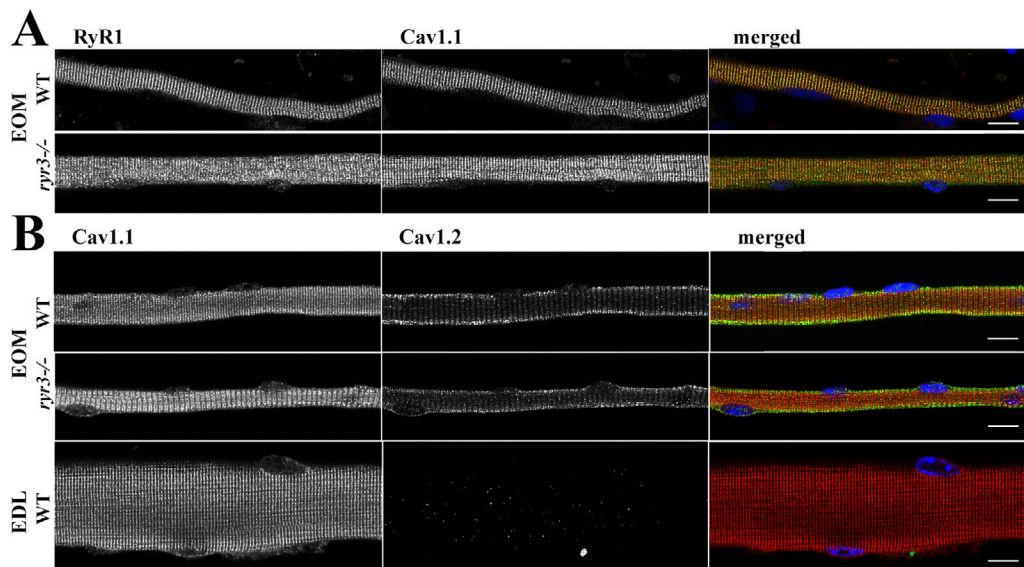


Figure 6. Immunohistochemical analysis and subcellular localization of RYR1 and of the $\alpha 1$ subunit of the DHPR in single muscle fibers from WT and *ryr3*^{-/-} mice. (A) Left and central panels show the staining obtained using rabbit anti-RYR1 mAb D4E1 (green in merged image) and mouse anti-Ca_v1.1 (red in merged image), respectively. The panel on the right shows the merged images as well as location of the myonuclei (DAPI, blue). **(B)** Left and central panels show the staining obtained using mouse anti-Ca_v1.1 (red in merged image) and rabbit anti-Ca_v1.2 (green in merged image), respectively. The panel on the right shows the merged images as well as location of the myonuclei (DAPI, blue). The bottom panels show staining of mouse EDL fibers, which are negative for Ca_v1.2 and were used as staining control. All images in B were acquired using the same settings for the laser intensities and acquisition parameters. Images were acquired using a Nikon A1 plus confocal microscope equipped with a Plan Apo 60 \times oil objective (numerical aperture, 1.4) and stained as described in Materials and methods. Orange pixels show areas of colocalization. Scale bars, 30 μ m.

with the Ca²⁺ indicator Mag-Fluo-4 (Fig. 7, A, B, D, and E) for measurements of electrically evoked Ca²⁺ transients or fura-2 (Fig. 7 C) for measurements of the resting cytoplasmic [Ca²⁺]. A representative trace of a Ca²⁺ transient elicited by field stimulation in EOM fibers from WT and *ryr3*^{-/-} mice is shown in Fig. 7 B. Detailed quantitative analysis revealed that the peak $\Delta F/F$ was similar in WT and *ryr3*^{-/-} EOM fibers (Fig. 7 D and Table 2), as was the TTP (Fig. 7 E and Table 2); however, the mean TTHP and HRTs were significantly slower in fibers from *ryr3*^{-/-} mice (Table 2). We would like to point out that these experiments were performed at room temperature (23–25°C), and thus, the absolute kinetic values *in vivo* may be faster (at 37°C) than those reported here. Nevertheless, the impact of ambient temperature on the Ca²⁺ kinetics of fibers from WT and *ryr3*^{-/-} should be the same. No significant difference was observed in the resting [Ca²⁺] (Fig. 7 C). Experiments were also performed to verify if EOM fibers exhibit sparks; 91 fibers from four WT mice were loaded with Fluo-4 (Lopez et al., 2016), but we failed to observe any spontaneous Ca²⁺ release events.

The results described so far indicate that RYR3 ablation causes specific alterations of intracellular calcium homeostasis

and could be responsible for the reduced visual capacity of the *ryr3*^{-/-} mice. However, the differences in calcium homeostasis observed between WT and *ryr3*^{-/-} mice could potentially be caused by changes in muscle development brought about by the absence of RYR3 rather than to changes in calcium fluxes due to the specific absence of the Ca²⁺ channel. This point is especially relevant, since (a) the expression of the RYR3 isoform peaks during development and decreases in mature muscles (Conti et al., 2005) and (b) in EOMs, but not in other skeletal muscles, there is a continuous process of myonuclear addition into normal uninjured adult myofibrils. The myonuclei derive from activated satellite cells residing within uninjured EOMs (McLoon and Wirtschafter, 2002a,b; Stuelsatz et al., 2015).

To address the subject of abnormal calcium homeostasis directly and bypass issues linked to development or muscle adaptation due to the lack of RYR3 in innervating neurons, we isolated satellite cells from EOMs, cultured them, and analyzed Ca²⁺ homeostasis in the resulting multinucleated myotubes (Fig. S2). No gross change in the number of myotubes or in their fusing capacity was observed. Furthermore, no significant changes in the resting Ca²⁺ concentration

Table 1. Colocalization analysis

	RYR1 \rightarrow Ca _v 1.1 overlap	Ca _v 1.1 \rightarrow RYR1 overlap	Ca _v 1.2 \rightarrow Ca _v 1.1 overlap	Ca _v 1.1 \rightarrow Ca _v 1.2 overlap
WT	0.801 \pm 0.126 (<i>n</i> = 5)	0.747 \pm 0.020 (<i>n</i> = 5)	0.479 \pm 0.051 (<i>n</i> = 5)	0.278 \pm 0.060 (<i>n</i> = 5)
<i>ryr3</i> ^{-/-}	0.677 \pm 0.068 (<i>n</i> = 4)*	0.647 \pm 0.082 (<i>n</i> = 4)*	0.378 \pm 0.127 (<i>n</i> = 4)	0.256 \pm 0.100 (<i>n</i> = 4)

Values represent mean \pm SD; *n* represents the number of fibers analyzed. n.s., not significant. *, *P* < 0.05, Student's *t* test.

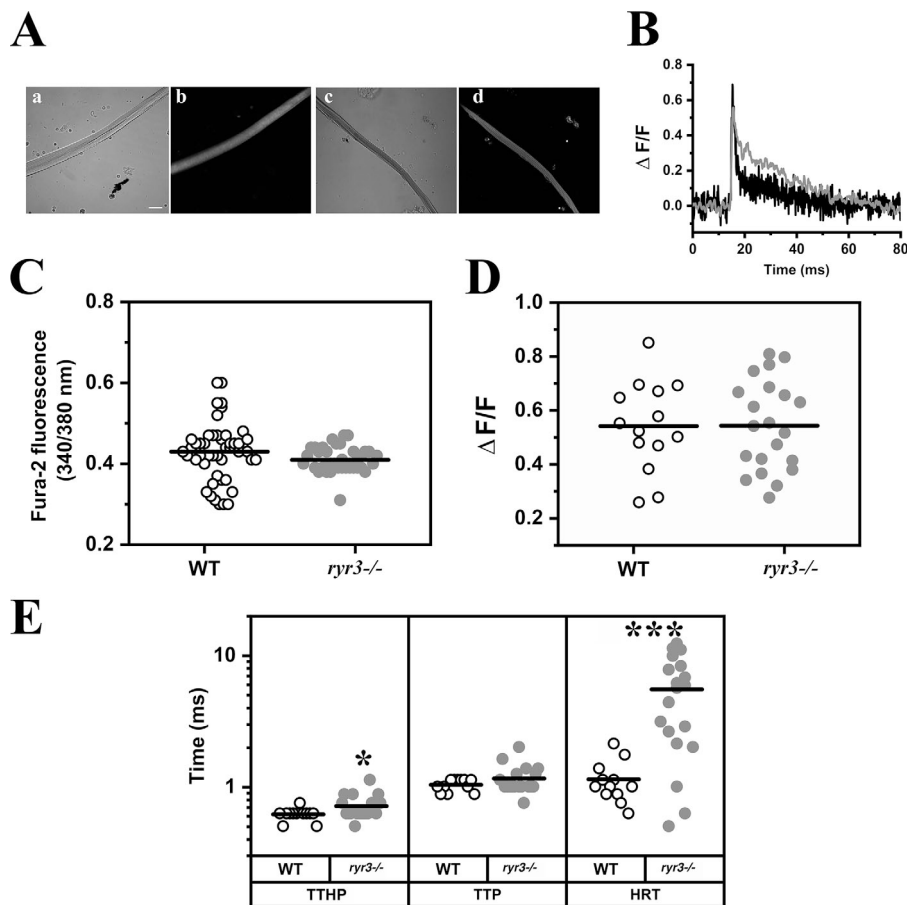


Figure 7. Calcium homeostasis in isolated EOM fibers. (A) Confocal images of WT (a and b) and *ryr3*^{-/-} (c and d) fibers; a and c show the transmitted light channel, and b and d show Mag-Fluo4 fluorescence, excited at 488 nm and recorded at an emission between 500 and 550 nm. Scale bar, 30 μ m. (B) Representative line scan traces of MagFluo4 calcium transients in EOM fibers from WT (black) and *ryr3*^{-/-} (gray), recorded at 7,921 lines per second. (C) Measurements of resting Ca²⁺ expressed as ratio (340/380 nm) using the fluorescent indicator fura-2. Each symbol represents the ratio obtained from a single fiber. The horizontal black line shows the mean value. Fibers were isolated from a total of three mice per group, and a total of 49 fibers from WT and 40 fibers from *ryr3*^{-/-} were analyzed. (D) Peak Ca²⁺ ($\Delta F/F$) of the MagFluo4 fluorescence obtained by stimulating EOM fibers by electrical field stimulation with a 0.5-ms bipolar pulse. All experiments were performed at room temperature. Each symbol represents the value from a single fiber. The horizontal black line shows the mean value. A total of 14 fibers from four WT mice and 21 fibers from nine *ryr3*^{-/-} mice were analyzed. (E) Analysis of the kinetics of the Ca²⁺ transients; TTHP, TTP, and HRT of the calcium transients are plotted. White dots, WT; gray dots, *ryr3*^{-/-}. A total of 12 fibers from four WT mice and 19 fibers from nine *ryr3*^{-/-} mice were analyzed. *, $P < 0.05$; ***, $P < 0.001$, Student's *t* test.

(86.6 \pm 3.2 nM vs. 95.3 \pm 5.1 nM in WT and *ryr3*^{-/-}, respectively; $n = 75$ cells) or the size of the rapidly releasable intracellular stores (3,210.0 \pm 539.6 vs. 2,548.5 \pm 180.7 arbitrary units in WT and *ryr3*^{-/-} respectively; $n = 9$) were observed. No Ca²⁺ sparks were detected in myotubes from WT or *ryr3*^{-/-} as determined with the calcium indicator Fluo-4. Interestingly, however, EOM-derived myotubes exhibited extremely rapid, repetitive Ca²⁺ oscillations that were more frequent in cells from WT than *ryr3*^{-/-} mice (Fig. 8, A–C). Additionally, the Ca²⁺ oscillations in *ryr3*^{-/-} myotubes were significantly slower than those observed in myotubes from WT mice (Fig. 8 D and Table 2).

Discussion

In the present report, we investigated the role of RYR3 in skeletal muscle by studying the biochemical and physiological characteristics of EOMs from *ryr3*^{-/-} mice. Knockout mice exhibited reduced visual capacity that is caused by a change in the physiological properties of the muscles, since (a) the mechanical properties of isolated muscles assessed in vitro were significantly different and (b) calcium homeostasis in single fibers and cultured myotubes explanted from EOMs was altered.

EOMs are subspecialized and highly complex muscles showing single and multiple innervations, as well as the presence of fibers with mixed fast- and slow-twitch contractile

Table 2. Analysis of the kinetics of the calcium transients in EOM fibers and myotubes from WT and *ryr3*^{-/-} mice

Type of Ca ²⁺ response	Genotype and cell type	Peak Ca ²⁺ (ΔF)	TTHP (ms)	TTP (ms)	HRT (ms)
Electrically evoked transient parameters	WT EOM fibers	0.458 \pm 0.036 ($n = 14$)	0.621 \pm 0.019 ($n = 12$)	1.042 \pm 0.032 ($n = 12$)	1.147 \pm 0.125 ($n = 12$)
	<i>ryr3</i> ^{-/-} EOM fibers	0.424 \pm 0.027 ($n = 21$)	0.718 \pm 0.034* ($n = 19$)	1.310 \pm 0.159 ($n = 19$)	5.531 \pm 0.877*** ($n = 19$)
Spontaneous Ca ²⁺ transient parameters	WT myotubes	0.506 \pm 0.003 ($n = 9,319$)	20.598 \pm 0.192 ($n = 9,319$)	29.885 \pm 0.347 ($n = 9,319$)	77.813 \pm 0.8138 ($n = 8,941$)
	<i>ryr3</i> ^{-/-} myotubes	0.6111 \pm 0.010**** ($n = 1,368$)	27.527 \pm 0.570**** ($n = 1,368$)	46.878 \pm 1.173**** ($n = 1,368$)	87.586 \pm 1.931**** ($n = 1,339$)

Experiments were performed at room temperature. Values represent mean \pm SEM. *, $P < 0.05$; ***, $P < 0.001$, Student's *t* test; *****, $P < 0.00001$, Welch's *t* test.

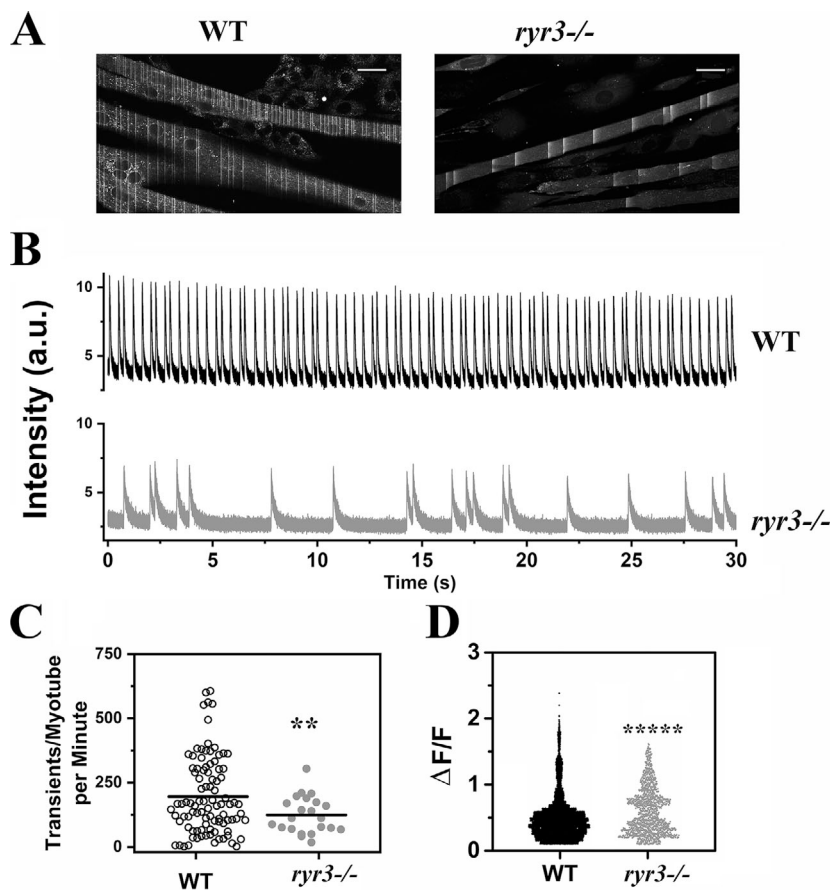


Figure 8. *ryr3*^{-/-} EOM-derived myotubes show fewer calcium waves than WT EOM-derived myotubes. **(A)** WT (left) and *ryr3*^{-/-} (right) confocal image of myotubes loaded with Fluo-4. Spontaneous calcium waves can be seen as lines during image acquisition. Scale bars, 30 μ m. **(B)** Representative Fluo-4 line scan traces of WT (top, black line) and *ryr3*^{-/-} (bottom, gray line) myotubes. a.u., arbitrary units. **(C)** Analysis of the frequency of the spontaneous Ca²⁺ transient. Each point represents the number of transients per minute recorded in a single myotube. Each myotube was recorded for 30 s, and the frequency output is given as frequency per minute. Experiments were performed at room temperature. The horizontal black line represents the mean value. Empty circles, WT ($n = 95$); gray circles, *ryr3*^{-/-} ($n = 22$). **(D)** $\Delta F/F$ of the Fluo-4 transients. The number of transients analyzed was $n = 9,319$ and $n = 1,368$ for WT and *ryr3*^{-/-}, respectively. **, $P < 0.005$; ****, $P < 0.0001$, Welch's t test.

characteristics within a single contracting unit (Mayr, 1971; Ketterer et al., 2010). We found that the absolute maximum force developed by mouse EOMs is ~ 10 times lower than that of other mouse limb muscles. In this study, because the size of mouse EOMs is very small (300–600 μ m diameter) and a small error in the cross-sectional area measurements would have a large impact on the corrected developed force, we displayed the absolute and noncorrected force values. The mechanical properties of EOMs from adult (12–16-wk-old) *ryr3*^{-/-} mice were different than those of WT mice. Indeed *ryr3*^{-/-} EOM developed less force and had slower kinetics (but did not show changes in muscle cross-sectional area). Such data are consistent with a previous report (Bertocchini et al., 1997) showing that diaphragm strips from 15-d-old *ryr3*^{-/-} mice stimulated at a frequency of 0.1 Hz developed less tension than their WT counterpart, though in muscles from adult mice, the differences disappeared.

The three- to fourfold slower half relaxation time observed in EOMs from *ryr3*^{-/-} mice would significantly impact the speed of the eye movement necessary for the mice to perform the requested visual tasks, and we are confident that such dramatic changes in force account for the decreased visual acuity detected in vivo. It should be pointed out that neither the OKR nor the cued water maze directly assess ocular muscle function. The OKR represents an automatic compensatory eye movement without any conscious effort to stabilize the image and responds when animals move about in a visual scene. This reflex requires

a visible retinal image and is particularly prominent in avoate animals (i.e., animals lacking the fovea; Stahl, 2004). Performing the cued water maze task also requires intact eyesight and motor ability (swimming and eye movement) to focus the visible platform located at different locations in the respective trials (Vorhees and Williams, 2006). Therefore, although no direct conclusions can be drawn and we cannot totally exclude an effect caused by neuronal RYR3 ablation, our results point toward an impact of RYR3 ablation on eye muscle function, especially since (a) no morphological and electrophysiological retinal differences between WT and *ryr3*^{-/-} animals were found, and (b) direct changes in the kinetics of the calcium signaling and velocity of contraction in isolated EOMs were found. We would also like to point out that *ryr3*^{-/-} mice were reported to exhibit impaired spatial learning as assessed by the Morris water maze and increased spontaneous open-field activity (Balschun et al., 1999). In view of the present findings, it is also possible that the reported spatial memory defects observed in *ryr3*^{-/-} mice were caused, at least in part, by altered ocular muscle function.

The reduced tension and speed of contraction observed in *ryr3*^{-/-} EOMs are most likely not caused by differences in the expression levels of ECC proteins and/or contractile proteins, since the expressed MyHC isoforms were similar in WT and *ryr3*^{-/-} EOMs and the ECC protein composition of total EOM extracts was similar in WT and transgenic mice. The small increase in the content of the calcium binding protein parvalbumin observed in *ryr3*^{-/-} EOMs cannot account for the changes in

the kinetics of relaxation. Indeed, a higher content of parvalbumin would be expected to increase the speed of relaxation and not prolong it (Heizmann et al., 1982; Müntener et al., 1995), indicating that the changes in the kinetic properties must be due to a different mechanism. Of interest, we did observe a significant reduction in the expression of RYR1 and CASQ1 transcripts, but this did not result in an overall change in their level of protein content.

Although it is difficult to directly determine the cause of the slow relaxation times of *ryr3*^{-/-} EOMs, they may relate to the location and physiological function of RYR3s. One possibility is that in murine EOMs, RYR3s are located parajunctionally, i.e., similar to their distribution in toadfish white swim muscle, frog sartorius, and 72 HPF zebrafish larvae (Felder and Franzini-Armstrong, 2002; Perni et al., 2015). This parajunctional subcellular localization could place the RYR3s adjacent to some SERCAs, whereby Ca²⁺ release via the parajunctional RYR3 would rapidly activate the Ca²⁺ pump, leading to a faster rate of relaxation. The lack of RYR3 would fail to rapidly activate the calcium ATPase, leading to a slower relaxation rate. Of note, close subcellular distribution of RYR3 and SERCA2a and of RYR2 and SERCA2b have also been reported in other tissues (Greene et al., 2000; Clark et al., 2010; Dally et al., 2010).

Since release of Ca²⁺ from intracellular stores is the driving force of skeletal muscle contraction, we hypothesized that the mechanism resulting in the changes in the mechanical properties of EOMs in the transgenic mice were due to alterations of Ca²⁺ release. In mammalian cells, RYR3s have been reported to reinforce CICR in developing murine skeletal muscles (Yang et al., 2001) and play a role in the duration and amplitude of osmotic shock-triggered Ca²⁺ sparks in adult skeletal muscle fibers (Weisleder et al., 2007). On the other hand, in non-mammalian skeletal muscles, RYR3s contribute both to the generation of sparks and to the Ca²⁺ transients (Zhou et al., 2003, 2004; Perni et al., 2015). Surprisingly, no sparks were observed in mouse EOM fibers, indicating that in the latter muscles spontaneous Ca²⁺ release events do not occur, possibly because of their particular expression of ECC protein machinery and dissimilar calcium homeostasis (Zeiger et al., 2010; Stuelsatz et al., 2015; Sekulic-Jablanovic et al., 2016). Interestingly, the kinetics of the Ca²⁺ transients (TTP and TTHP) in EOMs from WT mice were approximately four times faster than those reported using the same Ca²⁺ indicator in rat and mouse fast-twitch fibers. Indeed, in rat and mouse EDL fibers, the reported TTP of the Ca²⁺ transient was 4.6 ± 0.42 ms (Delbono and Stefani, 1993) and 4.4 ± 0.1 ms (Hollingworth et al., 2008), respectively, and the TTHP was 3.2 ± 0.1 ms, while in mouse EOMs, we calculated a TTP of 1.04 ± 0.03 ms and TTHP of 0.62 ± 0.02 ms. Thus, it is not only the presence of MyHC13, which is responsible for the superfast characteristics of EOM muscle contraction, but also their particular ECC machinery. Nevertheless, the observed changes of the Ca²⁺ transients between EOMs from WT and *ryr3*^{-/-} mice are clearly insufficient to account for the large changes in force development. The reduction in force may be due in part to the different preparations used to measure force and Ca²⁺ or to changes occurring during development. Indeed, EOMs from *ryr3*^{-/-} mice may have

physiologically adapted to the lack of RYR3 during muscle fiber maturation. To circumvent the possible alterations caused by modifications occurring during muscle fiber maturation, we studied Ca²⁺ homeostasis in myotubes obtained from satellite cells from adult EOMs and cultured and differentiated in vitro. Our results show that EOM-derived myotubes exhibit extremely rapid and repetitive Ca²⁺ oscillations, which occur in the absence of any exogenous stimulation and depend on extracellular Ca²⁺ (since they disappeared in Ca²⁺-free medium). More importantly, the velocity of the Ca²⁺ transients was 1.6 times slower in *ryr3*^{-/-} myotubes. The spontaneous oscillations were not completely abolished in myotubes from *ryr3*^{-/-} mice, but their number was substantially reduced, corroborating the role of RYR3 as a calcium signal amplifier. Though presently we do not know the function played by these Ca²⁺ oscillations, the lack of signals generated by their diminished activity potentially alters the myotubes, resulting in impaired regeneration of EOM.

In conclusion, our studies show that the lack of RYR3 has a significant impact on visual acuity by affecting the function of ocular muscles. It also suggests that in the future, mutations in RYR3 should be taken into consideration in patients with strabismus, ophthalmoplegia, and ptosis with or without involvement of the central nervous system.

Acknowledgments

The support of the Department of Anesthesia, Basel University Hospital and the technical support of Anne-Sylvie Monnet are gratefully acknowledged. We also thank Professors Stephan Frank and Jürgen Hench from the Institute for Medical Genetics and Pathology, Basel University Hospital for helpful discussions; Dr. Alexander Schmidt of the Proteomics Core Facility, Biozentrum Basel University, for performing the mass spectroscopy analysis; and Ms. Carolyn Trepp for help with the OKR experiments. We also acknowledge ARVO (copyright holder) for permission to reproduce Fig. 2 from Prusky et al., 2004.

This work was supported by the Swiss National Science Foundation (grant 31003A-169316), the OPO Stiftung (grant 2013/14-0038), and the Japan Society for the Promotion of Science (Core-to-core program).

The authors declare no competing financial interests.

Author contributions: J. Eckhardt designed and performed the experiments and analyzed the results with guidance from F. Zorzato and S. Treves; C. Bachmann performed the immunohistochemistry experiments on isolated fibers; M. Sekulic-Jablanovic performed the initial experiments on RYR3 expression in mouse EOMs as well as some of the in vivo visual experiments. V. Enzmann supported J. Eckhardt and M. Sekulic-Jablanovic in the in vivo visual experiments. J. Ma, K. Ho Park, and H. Takeshima constructed and supplied the *ryr3*^{-/-} mouse model. F. Zorzato and S. Treves designed the experiments on the mouse model, oversaw the project, and wrote the paper. All authors reviewed and helped elaborate the manuscript.

Eduardo Ríos served as editor.

Submitted: 24 January 2019

Accepted: 13 April 2019

References

- Airey, J.A., C.F. Beck, K. Murakami, S.J. Tanksley, T.J. Deerinck, M.H. Ellisman, and J.L. Sutko. 1990. Identification and localization of two triad junctional foot protein isoforms in mature avian fast twitch skeletal muscle. *J. Biol. Chem.* 265:14187–14194.
- Balschun, D., D.P. Wolfer, F. Bertocchini, V. Barone, A. Conti, W. Zuschratter, L. Missiaen, H.P.J. Lipp, J.U. Frey, and V. Sorrentino. 1999. Deletion of the ryanodine receptor type 3 (RyR3) impairs forms of synaptic plasticity and spatial learning. *EMBO J.* 18:5264–5273. <https://doi.org/10.1093/emboj/18.19.5264>
- Bers, D.M. 2002. Cardiac excitation-contraction coupling. *Nature.* 415: 198–205. <https://doi.org/10.1038/415198a>
- Bertocchini, F., C.E. Ovitt, A. Conti, V. Barone, H.R. Schöler, R. Bottinelli, C. Reggiani, and V. Sorrentino. 1997. Requirement for the ryanodine receptor type 3 for efficient contraction in neonatal skeletal muscles. *EMBO J.* 16:6956–6963. <https://doi.org/10.1093/emboj/16.23.6956>
- Brown, R.E., and A.A. Wong. 2007. The influence of visual ability on learning and memory performance in 13 strains of mice. *Learn. Mem.* 14:134–144. <https://doi.org/10.1101/lm.473907>
- Clark, J.H., N.P. Kinnear, S. Kalujnaia, G. Cramb, S. Fleischer, L.H. Jeyakumar, F. Wuytack, and A.M. Evans. 2010. Identification of functionally segregated sarcoplasmic reticulum calcium stores in pulmonary arterial smooth muscle. *J. Biol. Chem.* 285:13542–13549. <https://doi.org/10.1074/jbc.M110.101485>
- Conti, A., C. Reggiani, and V. Sorrentino. 2005. Selective expression of the type 3 isoform of ryanodine receptor Ca²⁺ release channel (RyR3) in a subset of slow fibers in diaphragm and cephalic muscles of adult rabbits. *Biochem. Biophys. Res. Commun.* 337:195–200. <https://doi.org/10.1016/j.bbrc.2005.09.027>
- Dally, S., E. Corvazier, R. Bredoux, R. Bobe, and J. Enouf. 2010. Multiple and diverse coexpression, location, and regulation of additional SERCA2 and SERCA3 isoforms in nonfailing and failing human heart. *J. Mol. Cell. Cardiol.* 48:633–644. <https://doi.org/10.1016/j.yjmcc.2009.11.012>
- de Chaumont, F., S. Dallongeville, N. Chenouard, N. Hervé, S. Pop, T. Provoost, V. Meas-Yedid, P. Pankajakshan, T. Lecomte, Y. Le Montagner, et al. 2012. Icy: an open bioimage informatics platform for extended reproducible research. *Nat. Methods.* 9:690–696. <https://doi.org/10.1038/nmeth.2075>
- Delbono, O., and E. Stefani. 1993. Calcium transients in single mammalian skeletal muscle fibres. *J. Physiol.* 463:689–707. <https://doi.org/10.1113/jphysiol.1993.sp019617>
- Delbono, O., J. Xia, S. Truetes, Z.M. Wang, R. Jimenez-Moreno, A.M. Payne, M.L. Messi, A. Briguet, F. Schaefer, M. Nishi, et al. 2007. Loss of skeletal muscle strength by ablation of the sarcoplasmic reticulum protein JP45. *Proc. Natl. Acad. Sci. USA.* 104:20108–20113. <https://doi.org/10.1073/pnas.0707389104>
- Endo, M. 1977. Calcium release from the sarcoplasmic reticulum. *Physiol. Rev.* 57:71–108. <https://doi.org/10.1152/physrev.1977.57.1.71>
- Enzmann, V., B.W. Row, Y. Yamauchi, L. Kheirandish, D. Gozal, H.J. Kaplan, and M.A. McCall. 2006. Behavioral and anatomical abnormalities in a sodium iodate-induced model of retinal pigment epithelium degeneration. *Exp. Eye Res.* 82:441–448. <https://doi.org/10.1016/j.exer.2005.08.002>
- Felder, E., and C. Franzini-Armstrong. 2002. Type 3 ryanodine receptors of skeletal muscle are segregated in a parajunctional position. *Proc. Natl. Acad. Sci. USA.* 99:1695–1700. <https://doi.org/10.1073/pnas.032657599>
- Franzini-Armstrong, C., and A.O. Jorgensen. 1994. Structure and development of E-C coupling units in skeletal muscle. *Annu. Rev. Physiol.* 56: 509–534. <https://doi.org/10.1146/annurev.ph.56.030194.002453>
- Giannini, G., E. Clementi, R. Ceci, G. Marziali, and V. Sorrentino. 1992. Expression of a ryanodine receptor-Ca²⁺ channel that is regulated by TGF- β . *Science.* 257:91–94. <https://doi.org/10.1126/science.1320290>
- Giannini, G., A. Conti, S. Mammarella, M. Scrobogna, and V. Sorrentino. 1995. The ryanodine receptor/calcium channel genes are widely and differentially expressed in murine brain and peripheral tissues. *J. Cell Biol.* 128:893–904. <https://doi.org/10.1083/jcb.128.5.893>
- Greene, A.L., M.J. Lalli, Y. Ji, G.J. Babu, I. Grupp, M. Sussman, and M. Periasamy. 2000. Overexpression of SERCA2b in the heart leads to an increase in sarcoplasmic reticulum calcium transport function and increased cardiac contractility. *J. Biol. Chem.* 275:24722–24727. <https://doi.org/10.1074/jbc.M001783200>
- Guiñón, J., E. Ortega, J. García-Antón, and V. Pérez-Herranz. 2007. Moving average and Savitzky-Golay smoothing filters using Mathcad. https://www.researchgate.net/publication/228407245_Moving_average_and_Savitzki-Golay_smoothing_filters_using_Mathcad
- Heizmann, C.W., M.W. Berchtold, and A.M. Rowlerson. 1982. Correlation of parvalbumin concentration with relaxation speed in mammalian muscles. *Proc. Natl. Acad. Sci. USA.* 79:7243–7247. <https://doi.org/10.1073/pnas.79.23.7243>
- Hoh, J.F.Y., S. Hughes, G. Hugh, and I. Pozgaj. 1989. Three hierarchies in skeletal muscle fibre classification: allotype, isotype and phenotype. In *UCLA Symposia on Molecular and Cellular Biology*. F. Stockdale, and L. Kedes, editors. Alan R. Liss, New York. 15–26.
- Hollingworth, S., U. Zeiger, and S.M. Baylor. 2008. Comparison of the myoplasmic calcium transient elicited by an action potential in intact fibres of mdx and normal mice. *J. Physiol.* 586:5063–5075. <https://doi.org/10.1113/jphysiol.2008.160507>
- Hollingworth, S., K.R. Gee, and S.M. Baylor. 2009. Low-affinity Ca²⁺ indicators compared in measurements of skeletal muscle Ca²⁺ transients. *Biophys. J.* 97:1864–1872. <https://doi.org/10.1016/j.bpj.2009.07.021>
- Hwang, H., K. Jung, Y. Takane, and T.S. Woodward. 2013. A unified approach to multiple-set canonical correlation analysis and principal components analysis. *Br. J. Math. Stat. Psychol.* 66:308–321. <https://doi.org/10.1111/j.2044-8317.2012.02052.x>
- Kaminski, H.J., and R.L. Ruff. 1997. Ocular muscle involvement by myasthenia gravis. *Ann. Neurol.* 41:419–420. <https://doi.org/10.1002/ana.410410402>
- Ketterer, C., U. Zeiger, M.T. Budak, N.A. Rubinstein, and T.S. Khurana. 2010. Identification of the neuromuscular junction transcriptome of extraocular muscle by laser capture microdissection. *Invest. Ophthalmol. Vis. Sci.* 51:4589–4599. <https://doi.org/10.1167/iovs.09-4893>
- Lopez, R.J., S. Byrne, M. Vukcevic, M. Sekulic-Jablanovic, L. Xu, M. Brink, J. Alamelu, N. Voermans, M. Snoeck, E. Clement, et al. 2016. An RYR1 mutation associated with malignant hyperthermia is also associated with bleeding abnormalities. *Sci. Signal.* 9:ra68. <https://doi.org/10.1126/scisignal.aad9813>
- Mayr, R. 1971. Structure and distribution of fibre types in the external eye muscles of the rat. *Tissue Cell.* 3:433–462. [https://doi.org/10.1016/S0040-8166\(71\)80045-9](https://doi.org/10.1016/S0040-8166(71)80045-9)
- McLoon, L.K., and J. Wirtschafter. 2002a. Activated satellite cells are present in uninjured extraocular muscles of mature mice. *Trans. Am. Ophthalmol. Soc.* 100:119–123, discussion:123–124.
- McLoon, L.K., and J.D. Wirtschafter. 2002b. Continuous myonuclear addition to single extraocular myofibers in uninjured adult rabbits. *Muscle Nerve.* 25:348–358. <https://doi.org/10.1002/mus.10056>
- Meissner, G. 2017. The structural basis of ryanodine receptor ion channel function. *J. Gen. Physiol.* 149:1065–1089. <https://doi.org/10.1085/jgp.201711878>
- Müntener, M., L. Käser, J. Weber, and M.W. Berchtold. 1995. Increase of skeletal muscle relaxation speed by direct injection of parvalbumin cDNA. *Proc. Natl. Acad. Sci. USA.* 92:6504–6508. <https://doi.org/10.1073/pnas.92.14.6504>
- Ogawa, Y., N. Kurebayashi, and T. Murayama. 2000. Putative roles of type 3 ryanodine receptor isoforms (RyR3). *Trends Cardiovasc. Med.* 10:65–70. [https://doi.org/10.1016/S1050-1738\(00\)00050-5](https://doi.org/10.1016/S1050-1738(00)00050-5)
- Ostertagova, E., and O. Ostertag. 2016. Methodology and Application of Savitzky-Golay Moving Average Polynomial Smoother. *Global J. Pure Appl. Math.* 12:3201–3210.
- Percival, A.L., A.J. Williams, J.L. Kenyon, M.M. Grinsell, J.A. Airey, and J.L. Sutko. 1994. Chicken skeletal muscle ryanodine receptor isoforms: ion channel properties. *Biophys. J.* 67:1834–1850. [https://doi.org/10.1016/S0006-3495\(94\)80665-4](https://doi.org/10.1016/S0006-3495(94)80665-4)
- Perni, S., K.C. Marsden, M. Escobar, S. Hollingworth, S.M. Baylor, and C. Franzini-Armstrong. 2015. Structural and functional properties of ryanodine receptor type 3 in zebrafish tail muscle. *J. Gen. Physiol.* 145: 173–184. <https://doi.org/10.1085/jgp.201411303>
- Porter, J.D., S. Khanna, H.J. Kaminski, J.S. Rao, A.P. Merriam, C.R. Richmonds, P. Leahy, J. Li, and F.H. Andrade. 2001. Extraocular muscle is defined by a fundamentally distinct gene expression profile. *Proc. Natl. Acad. Sci. USA.* 98:12062–12067. <https://doi.org/10.1073/pnas.211257298>
- Protasi, F., H. Takekura, Y. Wang, S.R. Chen, G. Meissner, P.D. Allen, and C. Franzini-Armstrong. 2000. RYR1 and RYR3 have different roles in the assembly of calcium release units of skeletal muscle. *Biophys. J.* 79: 2494–2508. [https://doi.org/10.1016/S0006-3495\(00\)76491-5](https://doi.org/10.1016/S0006-3495(00)76491-5)
- Prusky, G.T., N.M. Alam, S. Beekman, and R.M. Douglas. 2004. Rapid quantification of adult and developing mouse spatial vision using a virtual optomotor system. *Invest. Ophthalmol. Vis. Sci.* 45:4611–4616. <https://doi.org/10.1167/iovs.04-0541>
- Purves, D., G.J. Augustine, D. Fitzpatrick, L.C. Katz, A.S. LaMantia, J.O. McNamara, and S.M. Williams, editors. 2001. *Neuroscience*. Second

- edition. Sinauer Associates, Sunderland, MA. Available at: <https://www.ncbi.nlm.nih.gov/books/NBK10799/>.
- Ríos, E., and G. Pizarro. 1991. Voltage sensor of excitation-contraction coupling in skeletal muscle. *Physiol. Rev.* 71:849–908. <https://doi.org/10.1152/physrev.1991.71.3.849>
- Schägger, H., and G. von Jagow. 1987. Tricine-sodium dodecyl sulfate-polyacrylamide gel electrophoresis for the separation of proteins in the range from 1 to 100 kDa. *Anal. Biochem.* 166:368–379. [https://doi.org/10.1016/0003-2697\(87\)90587-2](https://doi.org/10.1016/0003-2697(87)90587-2)
- Schindelin, J., I. Arganda-Carreras, E. Frise, V. Kaynig, M. Longair, T. Pietzsch, S. Preibisch, C. Rueden, S. Saalfeld, B. Schmid, et al. 2012. Fiji: an open-source platform for biological-image analysis. *Nat. Methods.* 9: 676–682. <https://doi.org/10.1038/nmeth.2019>
- Sekulic-Jablanovic, M., A. Palmowski-Wolfe, F. Zorzato, and S. Treves. 2015. Characterization of excitation-contraction coupling components in human extraocular muscles. *Biochem. J.* 466:29–36. <https://doi.org/10.1042/BJ20140970>
- Sekulic-Jablanovic, M., N.D. Ullrich, D. Goldblum, A. Palmowski-Wolfe, F. Zorzato, and S. Treves. 2016. Functional characterization of orbicularis oculi and extraocular muscles. *J. Gen. Physiol.* 147:395–406. <https://doi.org/10.1085/jgp.201511542>
- Spencer, R.F., and J.D. Porter. 1988. Structural organization of the extraocular muscles. *Rev. Oculomot. Res.* 2:33–79.
- Stahl, J.S. 2004. Using eye movements to assess brain function in mice. *Vision Res.* 44:3401–3410. <https://doi.org/10.1016/j.visres.2004.09.011>
- Stuelsatz, P., A. Shearer, Y. Li, L.A. Muir, N. Ieronimakis, Q.W. Shen, I. Kirillova, and Z. Yablonska-Reuveni. 2015. Extraocular muscle satellite cells are high performance myo-engines retaining efficient regenerative capacity in dystrophin deficiency. *Dev. Biol.* 397:31–44. <https://doi.org/10.1016/j.ydbio.2014.08.035>
- Takeshima, H., S. Nishimura, T. Matsumoto, H. Ishida, K. Kangawa, N. Minamino, H. Matsuo, M. Ueda, M. Hanaoka, T. Hirose, and S. Numa. 1989. Primary structure and expression from complementary DNA of skeletal muscle ryanodine receptor. *Nature.* 339:439–445. <https://doi.org/10.1038/339439a0>
- Takeshima, H., T. Ikemoto, M. Nishi, N. Nishiyama, M. Shimuta, Y. Sugitani, J. Kuno, I. Saito, H. Saito, M. Endo, et al. 1996. Generation and characterization of mutant mice lacking ryanodine receptor type 3. *J. Biol. Chem.* 271:19649–19652. <https://doi.org/10.1074/jbc.271.33.19649>
- Talmadge, R.J., and R.R. Roy. 1993. Electrophoretic separation of rat skeletal muscle myosin heavy-chain isoforms. *J. Appl. Physiol.* 75:2337–2340. <https://doi.org/10.1152/jap.1993.75.5.2337>
- Thomas, B.B., M.J. Seiler, S.R. Satta, P.J. Coffey, and R.B. Aramant. 2004. Optokinetic test to evaluate visual acuity of each eye independently. *J. Neurosci. Methods.* 138:7–13. <https://doi.org/10.1016/j.jneumeth.2004.03.007>
- Treves, S., M. Vukcevic, P.Y. Jeannet, S. Levano, T. Girard, A. Urwyler, D. Fischer, T. Voit, H. Jungbluth, S. Lillis, et al. 2011. Enhanced excitation-coupled Ca²⁺ entry induces nuclear translocation of NFAT and contributes to IL-6 release from myotubes from patients with central core disease. *Hum. Mol. Genet.* 20:589–600. <https://doi.org/10.1093/hmg/ddq506>
- Vaithianathan, T., D. Narayanan, M.T. Asuncion-Chin, L.H. Jayakumar, J. Liu, S. Fleischer, J.H. Jaggar, and A.M. Dopico. 2010. Subtype identification and functional characterization of ryanodine receptors in rat cerebral artery myocytes. *Am. J. Physiol. Cell Physiol.* 299:C264–C278. <https://doi.org/10.1152/ajpcell.00318.2009>
- Vorhees, C.V., and M.T. Williams. 2006. Morris water maze: procedures for assessing spatial and related forms of learning and memory. *Nat. Protoc.* 1:848–858. <https://doi.org/10.1038/nprot.2006.116>
- Weisleder, N., C. Ferrante, Y. Hirata, C. Collet, Y. Chu, H. Cheng, H. Takeshima, and J. Ma. 2007. Systemic ablation of RyR3 alters Ca²⁺ spark signaling in adult skeletal muscle. *Cell Calcium.* 42:548–555. <https://doi.org/10.1016/j.ceca.2007.01.009>
- Yang, D., Z. Pan, H. Takeshima, C. Wu, R.Y. Nagaraj, J. Ma, and H. Cheng. 2001. RyR3 amplifies RyR1-mediated Ca²⁺-induced Ca_i release in neonatal mammalian skeletal muscle. *J. Biol. Chem.* 276:40210–40214. <https://doi.org/10.1074/jbc.M106944200>
- Zeiger, U., C.H. Mitchell, and T.S. Khurana. 2010. Superior calcium homeostasis of extraocular muscles. *Exp. Eye Res.* 91:613–622. <https://doi.org/10.1016/j.exer.2010.07.019>
- Zhou, J., G. Brum, A. Gonzalez, B.S. Launikonis, M.D. Stern, and E. Rios. 2003. Ca²⁺ sparks and embers of mammalian muscle. Properties of the sources. *J. Gen. Physiol.* 122:95–114. <https://doi.org/10.1085/jgp.200308796>
- Zhou, J., B.S. Launikonis, E. Ríos, and G. Brum. 2004. Regulation of Ca²⁺ sparks by Ca²⁺ and Mg²⁺ in mammalian and amphibian muscle. An RyR isoform-specific role in excitation-contraction coupling? *J. Gen. Physiol.* 124:409–428. <https://doi.org/10.1085/jgp.200409105>
- Zhou, Y., D. Liu, and H.J. Kaminski. 2010. Myosin heavy chain expression in mouse extraocular muscle: more complex than expected. *Invest. Ophthalmol. Vis. Sci.* 51:6355–6363. <https://doi.org/10.1167/jovs.10-5937>
- Zorzato, F., J. Fujii, K. Otsu, M. Phillips, N.M. Green, F.A. Lai, G. Meissner, and D.H. MacLennan. 1990. Molecular cloning of cDNA encoding human and rabbit forms of the Ca²⁺ release channel (ryanodine receptor) of skeletal muscle sarcoplasmic reticulum. *J. Biol. Chem.* 265: 2244–2256.
- Zorzato, F., A.A. Anderson, K. Ohlendieck, G. Froemming, R. Guerrini, and S. Treves. 2000. Identification of a novel 45 kDa protein (JP-45) from rabbit sarcoplasmic-reticulum junctional-face membrane. *Biochem. J.* 351:537–543.
- Zulliger, R., S. Lecaudé, S. Eigeldinger-Berthou, U.E. Wolf-Schnurrbusch, and V. Enzmann. 2011. Caspase-3-independent photoreceptor degeneration by N-methyl-N-nitrosourea (MNU) induces morphological and functional changes in the mouse retina. *Graefes Arch. Clin. Exp. Ophthalmol.* 249:859–869. <https://doi.org/10.1007/s00417-010-1584-6>